Journal of Power Sources 185 (2008) 828–837

Contents lists available at ScienceDirect

Journal of Power Sources

journal homepage: www.elsevier.com/locate/jpowsour

Optimum operating strategies for liquid-fed direct methanol fuel cells

Ilyong Jeong[a], Jiyong Kim[a], Sejin Pak[a], Suk Woo Nam[b], Il Moon[a,*]

[a] Department of Chemical Engineering, Yonsei University, 134 Sinchon-dong, Seodaemun-gu, Seoul 120-749, Republic of Korea
[b] Fuel Cell Research Center, Korea Institute of Science and Technology (KIST), P.O. Box 131, Cheongryang, Seoul 130-650, South Korea

ARTICLE INFO

Article history:
Received 18 April 2008
Accepted 25 June 2008
Available online 17 July 2008

Keywords:
Direct methanol fuel cell
Dynamic optimization
Start-up operation
Optimum operating strategies
Parameter estimation
Mathematical model

ABSTRACT

This study focuses on optimum operating strategies for liquid-fed direct methanol fuel cells (DMFCs) to minimize methanol consumption. A mathematical model is developed and verified with experimental data from the literature using the parameter estimation method. The model consists of a set of differential and algebraic equations and makes it possible to describe zero initial hold-up conditions. Based on the model, steady-state simulation results are obtained and explain the dependence on the feed concentration of key variables such as cell voltage, cell power density, overpotentials of both electrodes, and methanol crossover ratio. Dynamic simulation results are also presented to check the transient behaviour of a DMFC operated from start-up to shut-down. Dynamic optimization allows determination of the optimum transient strategies of feed concentration required to maximize the fuel efficiency. With six scenarios of power density load, it is demonstrated that the optimum transient strategies depend heavily on both the load of power density and the number of control actions. The main advantage of these approaches is to reduce fuel consumption and, ultimately, to enable DMFCs to be operated more efficiently.

1. Introduction

The direct methanol fuel cell (DMFC) is a hot research topic because it represents a power source for portable electronic and vehicular applications, employs a solid polymer electrolyte that works at relatively low temperature, and uses an inexpensive liquid fuel with an especially high specific energy. Methanol has a theoretical energy density of 6.1 Wh g^{-1}. Even a 20% efficient DMFC is more than three times efficient than advanced lithium batteries [1]. Nevertheless, in practice, DMFC suffers from two intrinsic drawbacks. One is the slow reaction kinetics of the methanol oxidation in the catalyst layer of the negative electrode (anode) because of the complexity of its mechanism. This results in a much lower open-circuit voltage (OCV) than is seen with other types of fuel cells, such as the hydrogen proton-exchange membrane fuel cell (PEMFC), and, consequently, a far lower power generation for a given size. The other drawback is that methanol permeates into the proton-exchange membrane (PEM) to reach the cathode catalyst layer, where it forms a mixed potential that decreases the cell voltage. This phenomenon, termed methanol crossover, not only results in a waste of fuel but also degrades the performance of the fuel cell [2]. It is thus very important to predict methanol crossover and to find operating strategies that can reduce methanol crossover, so as to improve system efficiency.

Recently, extensive studies have been carried out to predict methanol crossover in DMFCs; such studies have employed not only experimental methods [1–7] but also modelling systems [8–15]. Danilov et al. [8] developed a three-dimensional, two-phase CFD model to predict the internal phenomena of a DMFC. Sundmacher et al. [9] and Zhou et al. [10] formulated a dynamic differential and algebraic equations (DAEs)-based model and simulated cell voltage response to dynamic changes of methanol feed concentration in order to determine whether periodically pulsed methanol feeding could reduce methanol crossover. These authors used an anodic reaction mechanism that consisted of four steps, and derived an analytical solution of anodic reaction rate, assuming the first reaction step to be rate-determining. Jeng and Chen [11] developed a one-dimensional steady-state model on the anode side of the DMFC and found that methanol crossover became serious at low current density and high methanol concentration. Schultz and Sundmacher [12] improved on their previous work [9,10] with a partially one-dimensional dynamic model to characterize the flow directional behaviour in the PEM and diffusion layers. Krewera and Sundmacher [13] applied transfer function analysis to investigations of the dynamic behaviour of DMFCs. They investigated cell voltage responses to cell current step changes, and developed a criterion for cell voltage overshooting.

Another approach to modelling is dynamic optimization to find the optimum operating conditions, which was first addressed by Xu

* Corresponding author. Tel.: +82 2 2123 2761; fax: +82 2 312 6401.
E-mail address: ilmoon@yonsei.ac.kr (I. Moon).

0378-7753/$ – see front matter © 2008 Elsevier B.V. All rights reserved.
doi:10.1016/j.jpowsour.2008.06.095

Nomenclature

A^S	cross-sectional electrode area (m^2)
c_i	concentration of component i in the anode compartment ($mol\,m^{-3}$)
c_i^{CL}	concentration of component i in the anode catalyst layer ($mol\,m^{-3}$)
c_i^{Feed}	feed concentration of component i ($mol\,m^{-3}$)
C_j	double layer capacity of the electrode j ($F\,m^{-2}$)
d^M	thickness of the membrane (m)
D^M_{MeOH}	diffusion coefficient of methanol in the membrane ($m^2\,s^{-1}$)
F	Faraday's constant (96,485 $C\,mol^{-1}$)
i_{cell}	cell current density ($A\,m^{-2}$)
k_j	reaction rate constant of the electrode j ($mol\,m^{-2}\,s^{-1}$)
k^{LS}	mass transfer coefficient ($m\,s^{-1}$)
n_i^M	mass flux of component i in the membrane ($mol\,m^{-2}\,s^{-1}$)
p_j	pressure of the electrode j (Pa)
r_j	reaction rate of the electrode j ($mol\,m^{-2}\,s^{-1}$)
R	universal gas constant (8.314 $J\,mol^{-1}\,K^{-1}$)
t	time (s)
T	temperature (K)
U_{cell}	cell voltage (V)
U^{STD}_{cell}	standard cell voltage (1.21 V)
v^M	superficial velocity of water in the membrane ($m\,s^{-1}$)
V_a	volume of the anode compartment (m^3)
V^F	anode feed flow rate ($m^3\,s^{-1}$)
V_a^{CL}	volume of the anode catalyst layer (m^3)
x_i^{CL}	mole fraction of component i in the anode catalyst layer

Greek letters

α_j	charge transfer coefficient of the electrode j
ε_j^{CL}	void fraction of catalyst layer of the electrode j
η_j	overpotential of the electrode j (V)
κ^M	conductivity of the membrane ($\Omega^{-1}\,m^{-1}$)

Subscripts

a	anode
c	cathode
CO_2	carbon dioxide
MeOH	methanol

Superscripts

CL	catalyst layer
Feed	feed
M	membrane (PEM)
STD	at standard conditions

et al. [14]. They maximized the integration of cell voltage over the entire time domain under constant cell current density and adopted the model of Sundmacher et al. [9] to obtain the optimum feed concentration. More practical optimization work was performed by Ko et al. [15], who developed a non-isothermal dynamic optimization model based on the isothermal model of Sundmacher et al. [9] and optimized the fuel efficiency satisfying the power load. According to their results, of the three operating variables, namely, the methanol concentration, feed flow rate at the anode, and air flow rate at the cathode, the feed concentration has the strongest influence on the dynamic behaviour of a DMFC.

In this research, we focus on the identification of the optimum operating strategies of DMFCs over their entire operating procedure, including start-up operation. In the initial state of the start-up operation, the cell is assumed to be fully hydrated; it contains neither methanol nor carbon dioxide. In order to simulate and optimize the start-up operation, it is necessary to consider zero initial hold-up conditions for methanol and carbon dioxide in the dynamic model of DMFC, even though these conditions tend to cause unexpected numerical problems. In contrast to previous contributions to the dynamic optimization of DMFCs [14,15], the present study adopts zero initial hold-up conditions to describe the early state of the start-up operation.

2. Mathematical model

The focus of the research is a single cell of a DMFC. As shown in Fig. 1, the cell consists of a membrane electrode assembly (MEA) and anode and cathode flow-fields with a symmetric structure that centres on a PEM. The MEA can be divided into five layers: a PEM, two catalyst layers, and two diffusion layers. The PEM separates the anode side from the cathode side; ideally, it allows proton transport only. A dilute solution of methanol (typically less than 2 M for the active type, and about 5 M for the passive type) is fed to the anode flow channel; air or pure oxygen is supplied to the cathode side. The feeds permeate the diffusion layers and reach the catalyst layers. At the anode catalyst layer, 1 mol of methanol reacts with an equimolar amount of water to produce 1 mol of carbon dioxide and 6 mol of protons and electrons. By contrast, at the cathode catalyst layer, 1.5 mol of oxygen react with 6 mol of protons and electrons to produce 3 mol of water.

2.1. Assumptions and conditions

The aim is to develop a rigorous dynamic model to describe and analyze the dynamic behaviour of a DMFC. The model is a modification of those of Sundmacher et al. [9] and Zhou et al. [10], and considers material transports and electrochemical reactions under the following assumptions and conditions.

- The system is treated as a continuous stirred tank reactor (CSTR) that is operated isothermally.
- The diffusion layers and the flow fields are combined into the compartments.
- Ohmic drops in current-collectors and electric connections are negligible.
- Oxygen is supplied in excess and therefore no oxygen mass balance is required.
- The PEM is fully hydrated and allows for transport of protons and methanol only.
- The water concentration is constant (excess component in liquid mixture).
- Mass transport resistances in the catalyst layers are negligible because these are thin in comparison with the diffusion layers and PEM.
- The mass transport coefficients of methanol and carbon dioxide are equal.
- The electrochemical reactions of the anode and the cathode catalyst layers follow the Butler–Volmer reaction mechanism.
- The mixtures in the system are treated as pure liquid phase mixtures, i.e., gas-phase formation by release of carbon dioxide bubbles is not considered.

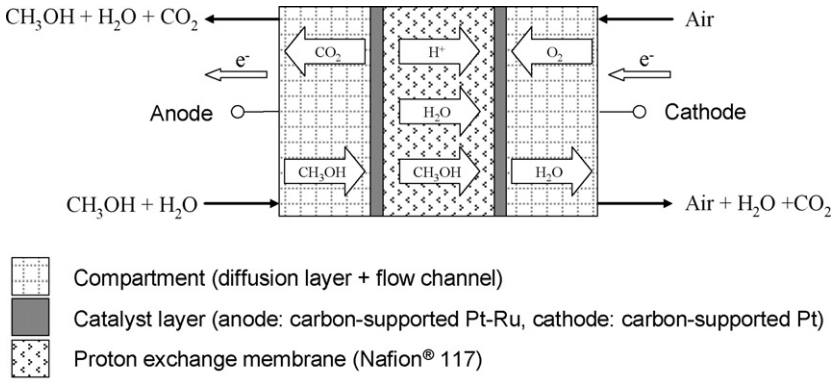

$$\text{Anode: } CH_3OH(l) + H_2O(l) \xrightarrow{Pt/Ru} CO_2(g) + 6H^+ + 6e^- \quad U^{\theta}_{MeOH\leftrightarrow CO_2} = 0.02\ V$$

$$\text{Cathode: } \tfrac{3}{2}O_2(g) + 6H^+ + 6e^- \xrightarrow{Pt} 3H_2O(l) \quad U^{\theta}_{O_2\leftrightarrow H_2O} = 1.23\ V$$

$$\text{Overall: } CH_3OH(l) + \tfrac{3}{2}O_2(g) \longrightarrow CO_2(g) + 2H_2O(l) \quad U^{\theta}_{Cell} = 1.21\ V$$

Fig. 1. Basic structure and reaction scheme of DMFC.

2.2. Model equations

In the anode compartment, methanol is fed to reach the anode catalyst layer, and carbon dioxide comes from the anode catalyst layer. The material balances of methanol and carbon dioxide in the anode compartment can be written as

$$\frac{dc_{MeOH}}{dt} = \frac{V^F}{V_a}(c^{Feed}_{MeOH} - c_{MeOH}) - \frac{k^{LS}A^S}{V_a}(c_{MeOH} - c^{CL}_{MeOH}) \quad (1)$$

$$\frac{dc_{CO_2}}{dt} = \frac{V^F}{V_a}(c^{Feed}_{CO_2} - c_{CO_2}) - \frac{k^{LS}A^S}{V_a}(c_{CO_2} - c^{CL}_{CO_2}) \quad (2)$$

In the anode catalyst layer, methanol from the anode compartment is consumed by methanol crossover as well as by electrochemical reaction producing equimolar carbon dioxide:

$$\frac{dc^{CL}_{MeOH}}{dt} = \frac{k^{LS}A^S}{V^S_a}(c_{MeOH} - c^{CL}_{MeOH}) - \frac{A^S}{V^{CL}_a}(n^M_{MeOH} + r_a) \quad (3)$$

$$\frac{dc^{CL}_{CO_2}}{dt} = \frac{k^{LS}A^S}{V^{CL}_a}(c_{CO_2} - c^{CL}_{CO_2}) + \frac{A^S}{V^{CL}_a}r_a \quad (4)$$

It is well known that the mechanism of the electrochemical reactions in a DMFC is complicated and utilizes several intermediate reactions [9,10]. To reduce the number of unknown parameters, however, this research adopts Butler–Volmer-type equations for the rate expressions of methanol oxidation at the anode catalyst layer and oxygen reduction at the cathode catalyst layer, i.e.,

$$r_a = k_a\left(x^{CL}_{MeOH}\ \exp\left(\frac{\alpha_a F}{RT}\eta_a\right) - x^{CL}_{CO_2}\exp\left(-\frac{(1-\alpha_a)F}{RT}\eta_a\right)\right) \quad (5)$$

$$r_c = k_c\left(\left(\frac{p_{O_2}}{p^{STD}}\right)^{1.5}\exp\left(-\frac{\alpha_c F}{RT}\eta_c\right) - \exp\left(\frac{(1-\alpha_c)F}{RT}\eta_c\right)\right) \quad (6)$$

where x^{CL}_i is the mole fraction of component i (methanol, carbon dioxide and water) and p_{O_2} is the partial pressure of oxygen in the cathode catalytic layer. At the anode side, six protons and electrons are produced from the methanol oxidation; at the cathode side, four protons and electrons are produced from the undesired methanol oxidation due to methanol crossover ($CH_3OH + 0.5O_2 \rightarrow CO_2 + 4H^+ + 4e^-$), whereas six protons and electrons are consumed by oxygen reduction. The charge balances of anode and cathode sides are therefore given by

$$\frac{d\eta_a}{dt} = \frac{1}{C_a}(i_{cell} - i_a) = \frac{1}{C_a}(i_{cell} - 6Fr_a) \quad (7)$$

$$\frac{d\eta_c}{dt} = \frac{1}{C_c}(-i_{cell} - i_c) = \frac{1}{C_c}(-i_{cell} - 6Fr_c + 4Fn^M_{MeOH}) \quad (8)$$

Assuming that the PEM is fully hydrated and the total flux through the PEM is almost the same as the flux of water (only because the concentration of methanol is extremely low in the DMFC), Jeng and Cheng [11] derived the rate of methanol crossover as follows:

$$n^M_{MeOH} = \frac{c^{CL}_{MeOH}v^M\exp(v^M d^M/D^M_{MeOH})}{(\exp(v^M d^M/D^M_{MeOH}) - 1)} \quad (9)$$

where v^M is the superficial velocity of water in the PEM, which can be calculated by

$$v^M = \frac{M_{H_2O}\lambda_{H_2O}}{\rho_{H_2O}}\left(\frac{i_{cell}}{F}\right) \quad (10)$$

The overall cell voltage is a function of the open-circuit voltage (OCV), anode and cathode overpotentials, and ohmic loss in the PEM:

$$U_{cell} = U^{STD}_{cell} - \eta_a + \eta_c - \frac{d^M}{\kappa^M}i_{cell} \quad (11)$$

When the cell is operated under galvanostatic conditions, the overall cell voltage can be calculated if only two overpotentials are obtained.

To simulate the cell using Eqs. (1)–(11), it is necessary to find several physical properties especially on the PEM (Nafion® 117). They are usually expressed as a function of temperature. The diffusivity of methanol in the PEM, D^M_{MeOH} in Eq. (9), is known to be a function of temperature [16], namely:

$$D^M_{MeOH} = D^M_{MeOH,ref}\exp\left(\frac{\Delta E}{R}\left(\frac{1}{T_{ref}} - \frac{1}{T}\right)\right) \quad (12)$$

Scott et al. [16] reported that Springer et al. [17] obtained a value of 2436 K for $\Delta E/R$ that pertains to measurements on Nafion® 117. For a reference value, Kauranen and Skou [18] measured a superficial diffusivity of methanol in the PEM of 4.9×10^{-10} m^2 s^{-1} at 60 °C. Finally, the diffusivity of methanol in the PEM at temperature T can

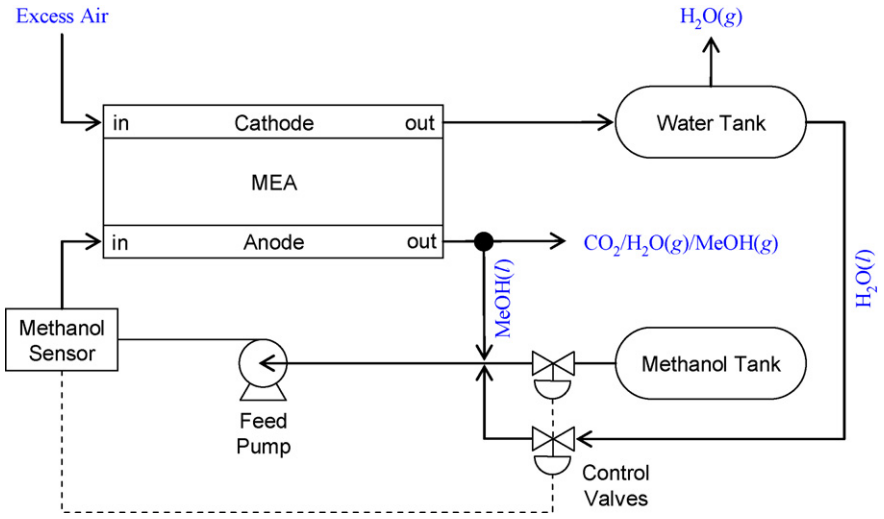

Fig. 2. Target system for dynamic operation of DMFC.

be calculated by:

$$D^{M}_{MeOH} = 4.9 \times 10^{-10} \exp\left(2436\left(\frac{1}{333} - \frac{1}{T}\right)\right) \quad (13)$$

The temperature dependence of the electro-osmotic drag coefficient of water (λ_{H_2O} in Eq. (10)) in fully hydrated PEM can be estimated from the experimental data of Ren et al. [19] by regression analysis using an exponential growth function with three parameters:

$$\lambda_{H_2O} = -0.0382 + 0.1585 \exp(8.7129 \times 10^{-3}\,T) \quad (14)$$

Springer et al. [17] obtained the ionic conductivity of Nafion® 117 as a function of temperature and water content ψ:

$$\kappa^{M} = (0.5139\psi - 0.326) \exp\left(1268\left(\frac{1}{303} - \frac{1}{T}\right)\right) \quad (15)$$

The water content (ψ) of the membrane is defined as the ratio of the number of water molecules to the number of SO_3^- groups per volume unit. Dohle et al. [20] presented the water content of the membrane as a function of the relative humidity, which is defined as the ratio of the partial pressure of water to the saturated pressure of water. Siebke et al. [21] reported a more convenient equation, which depends only on temperature and assumes that the membrane is fully hydrated:

$$\psi = 9.38 + 0.138(T - 273.15) \quad (16)$$

Table 1
Operating conditions and parameters

Parameter	Value
Operating conditions	
Anode inlet pressure, P_a (Pa)	101,325
Cathode inlet pressure, P_c (Pa)	303,975
Operating Temperature, T (K)	343.15
Anode feed flow rate, V^F ($\times 10^{-8}$ m^3 s^{-1})	2.267
Geometric parameters	
Cross-sectional electrode area, A^S ($\times 10^{-4}$ m^2)	9
Volume of anode compartment, V_a ($\times 10^{-6}$ m^3)	2
Porosity of anode catalyst layer, ε	0.81
Thickness of PEM, d^M ($\times 10^{-6}$ m)	200
Thickness of catalyst layer, d^{CL} ($\times 10^{-6}$ m)	10
Thickness of diffusion layer, d^{DL} ($\times 10^{-6}$ m)	100
Design parameters	
Double layer capacity of anode, C_a ($\times 10^5$ F m^{-2})	4
Double layer capacity of cathode, C_c ($\times 10^5$ F m^{-2})	8
Standard cell voltage, U^{STD}_{cell} (V)	1.21
Standard pressure, P^{STD} (Pa)	101,325
Universal constants	
Gas constant, R (J mol^{-1} K^{-1})	8.314
Faraday's constant, F (C mol^{-1})	96,485
Physical properties	
Molecular weight of water, M_w (kg mol^{-1})	0.018
Molar concentration of water, c_{H_2O} (mol m^{-3})	55,556

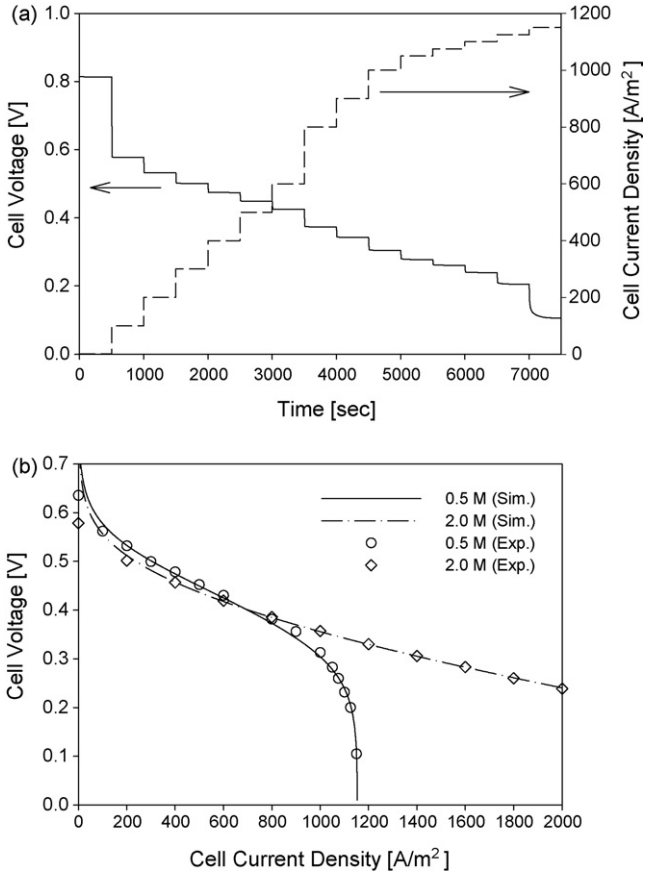

Fig. 3. (a) Dynamic response of cell voltage to step change of cell current density when feed concentration of methanol is set to 500 mol m^{-3} and (b) predicted polarization curves with experimental data [9].

Table 2
Summary of parameter estimation results

Parameter	Unit	Initial guess	Estimated value
Anode charge transfer coefficient, α_a	–	0.5	0.6033
Cathode charge transfer coefficient, α_c	–	0.5	0.3756
Rate constant of anodic reaction, k_a	mol m^{-2} s^{-1}	5×10^{-6}	2.159×10^{-7}
Rate constant of cathodic reaction, k_c	mol m^{-2} s^{-1}	1×10^{-2}	2.285×10^{-3}
Mass transfer coefficient, k^{LS}	m s^{-1}	1×10^{-5}	4.737×10^{-6}

Combining Eqs. (15) and (16), the ionic conductivity is obtained as a function of temperature:

$$\kappa^{M} = (0.0709T - 14.88)\ \exp\left(1268\left(\frac{1}{303} - \frac{1}{T}\right)\right) \quad (17)$$

The density of water in Eq. (10) depends on the temperature:

$$\ln \rho_{H_2O} = \sum_{i=1}^{6} a_i (T - T_{ref})^{i-1} \quad (18)$$

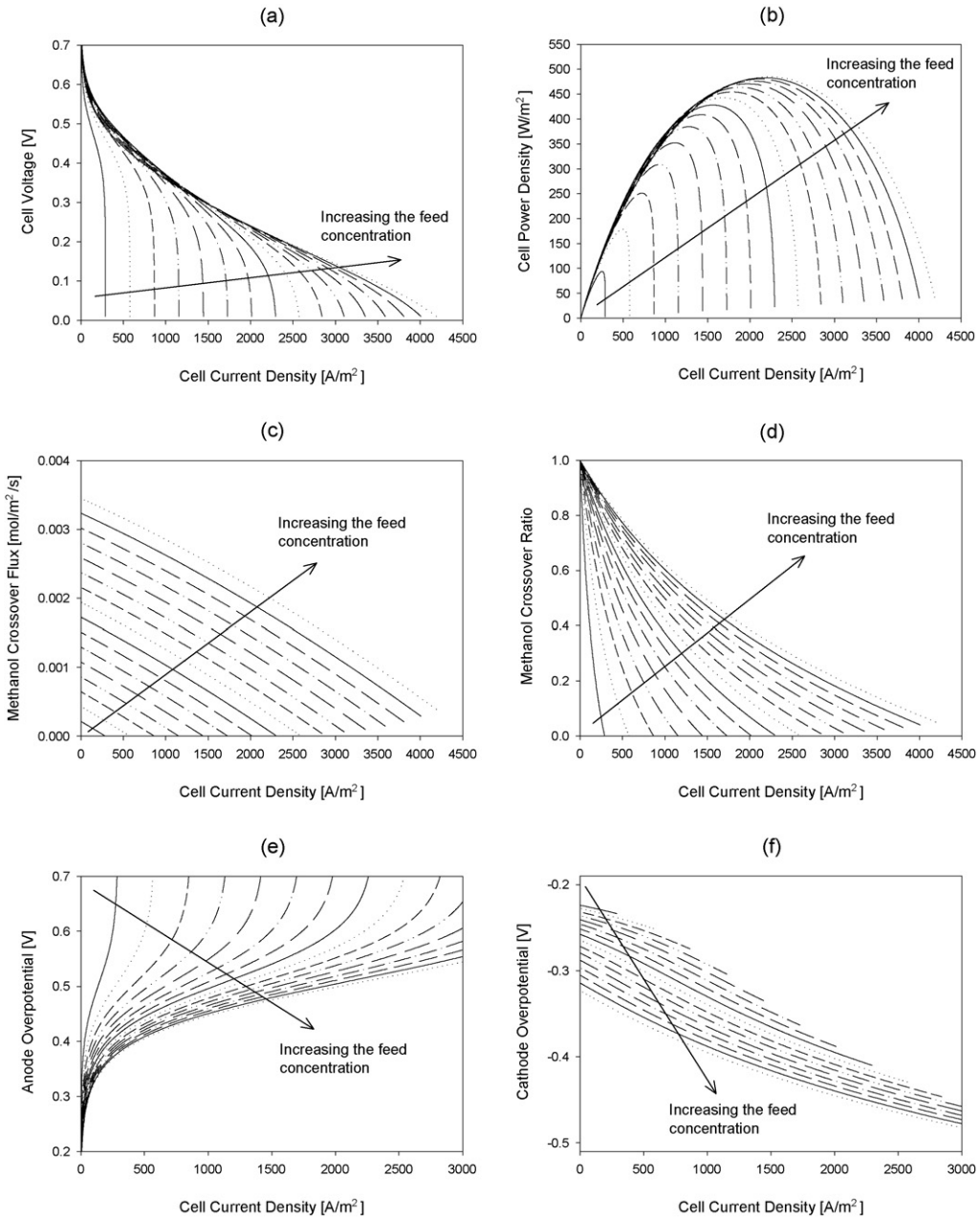

Fig. 4. Steady-state simulation results according to feed concentration of methanol from 0.125 to 2 M with interval of 0.125: (a) polarization curves; (b) power–current curves, (c) methanol crossover fluxes; (d) methanol crossover ratios; (e) anode overpotentials; (f) cathode overpotentials.

where the six coefficients are 6.9094, -2.0146×10^{-5}, -5.9868×10^{-6}, 2.5921×10^{-8}, -9.3244×10^{-11}, and 1.2103×10^{-13}, respectively, and the reference temperature (T_{ref}) is 273 K.

The mathematical model involves six differential equations; thus the same number of initial conditions are required:

$$c_{MeOH}|_{t=0} = c_{MeOH}^{init}, \quad c_{CO_2}|_{t=0} = c_{CO_2}^{init}, \quad c_{MeOH}^{CL}|_{t=0} = c_{MeOH}^{CL,init},$$
$$c_{CO_2}^{CL}\big|_{t=0} = c_{CO_2}^{CL,init}, \quad r_c|_{t=0} = r_c^{init}, \quad U_{cell}|_{t=0} = U_{cell}^{init} \tag{19}$$

where the superscript 'init' means the initial value. Since zero initial hold-up conditions are considered in this research, the initial hold-ups of methanol and carbon dioxide in the anode compartment and anode catalyst layer will be zero.

2.3. Target system

To describe the dynamic operation of a DMFC, the system that consists not only of the cell but also the accessories, such as the feed pump, storage tanks and control valves with the methanol sensor, as shown in Fig. 2. Initially, 2 M methanol and pure water are stored in the methanol and water tanks, respectively. A sensor detects the methanol concentration, sends a signal to the control valves connected to the water and methanol tanks, and finally permits control of the feed concentration from 0 to 2 M. It is assumed that the output concentration of methanol ($c_{MeOH}^{Feed,out}$) shows a first-order response to the input change ($c_{MeOH}^{Feed,in}$) in a piecewise constant fashion:

$$\tau \frac{dc_{MeOH}^{Feed,out}}{dt} + c_{MeOH}^{Feed,out} = K c_{MeOH}^{Feed,in} \tag{20}$$

where τ is the time constant and K is the steady-state gain. The feed pump supplies the cell with methanol solution at a constant flow rate. The operating conditions and parameters are summarized in Table 1.

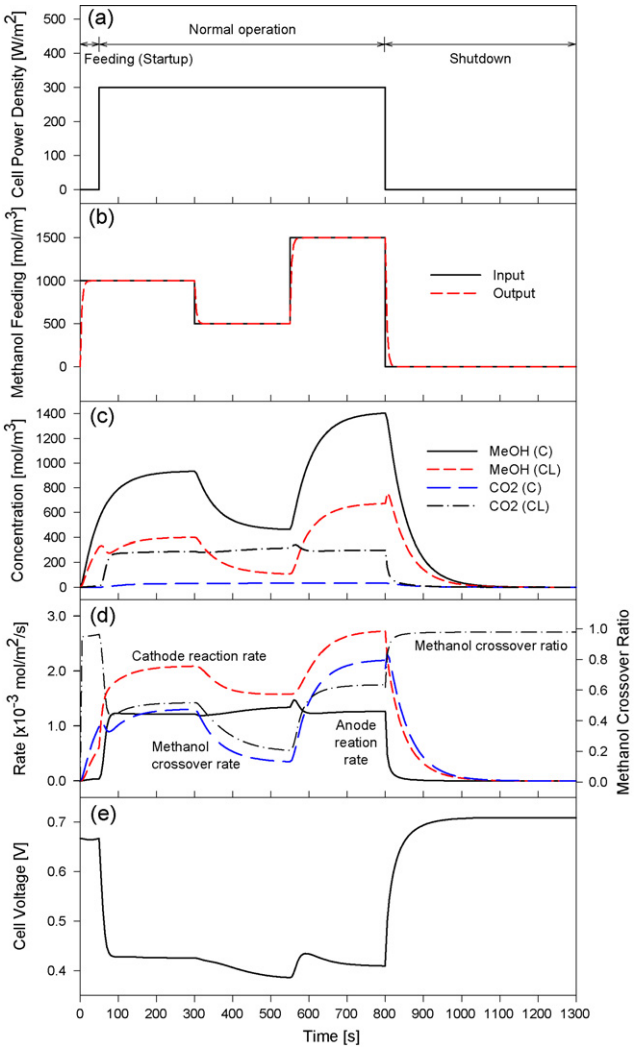

Fig. 5. Transient behaviour of DMFC: (a) scenario for power density load; (b) input and output concentrations of methanol feeding; (c) concentration profiles of methanol and carbon dioxide in anode compartment (C) and in anode catalyst layer (CL); (d) reaction rates and methanol crossover flux (left axis) and methanol crossover ratio (right axis); (e) cell voltage profiles.

2.4. Parameter estimation

To verify the model, five parameters were selected from the model equations, namely: the charge transfer coefficients of the anode and cathode (α_a, α_c), the reaction rate constants of the anode and cathode (k_a, k_c), and the mass transfer coefficient (k^{LS}). The parameter estimation was performed in the same way as the experimental method shown in Fig. 3a. It minimizes the difference between the experimental data and the cell voltage responses to the piecewise constant inputs of the cell current density to find the best-solution set of selected parameters. The optimization model for the parameter estimation can be formulated as

$$\min_{\pi_i \in \Pi} \sum_{k=1}^{K} \sum_{j=1}^{J} \left[\ln(\sigma_{jk}^2) + \frac{(U_{cell,jk}^{est} - U_{cell,jk}^{exp})^2}{\sigma_{jk}^2} \right]$$
$$\text{s.t. } f(x(t), \dot{x}(t), y(t), v)=0,$$
$$I(x(0), \dot{x}(0), y(0), v)=0,$$
$$\pi_i^L \le \pi_i \le \pi_i^U \tag{21}$$

here Π (the set of parameters to be estimated) = $\{\alpha_a, \alpha_c, k_a, k_c, k^{LS}\}$ and all of parameters have their own boundaries; L and U denote the lower and upper boundaries, respectively. The symbols f and I represent the model equations discussed in the previous section, and the initial conditions for differential equations. Each experiment k has J_k piecewise constant inputs of cell current density. σ_{jk}^2 is the variance of the jth step input of the cell current density in experiment k. For a variance model, the heteroscedastic variance model was chosen, i.e.,

$$\sigma^2 = \omega^2 (U_{cell}^2 + \varepsilon)^{\gamma} \tag{22}$$

where ε is the absolute tolerance and has a fixed value of 1×10^{-5}. Two parameters, ω and γ, will be determined from the optimization under their lower and higher boundaries. To estimate the selected five parameters, we used the estimation module in gPROMS [22,23] and two sets of experimental data for methanol feed concentrations of 500 and 2000 mol m^{-3} from Sundmacher et al. [9]. The polarization curves from the estimation results show good agreement with the experimental data, as seen in Fig. 3b. The R^2 values of the two

Table 3
Six scenarios generated for the case study

Scenario No.	Step 1	Step 2	Step 3	Step 4
1	Feeding	High	Normal	Low
2	Feeding	Normal	High	Low
3	Feeding	High	Low	Normal
4	Feeding	Low	High	Normal
5	Feeding	Normal	Low	High
6	Feeding	Low	Normal	High
Step time (s)	60	600	600	600

cases are 0.946 and 0.902, respectively. The parameter estimation results are summarized in Table 2.

3. Model verification

3.1. Steady-state results

Fig. 4 presents the steady-state cell performances based on the feed concentration of methanol. Six variables are plotted against cell current density: (i) cell voltage, (ii) cell power density, (iii) methanol crossover flux, (iv) methanol crossover ratio, (v) anode overpotential, and (vi) cathode overpotential. Each figure thus has 16 graphs, and they match to the feed concentration of methanol from 0.125 to 2 M, with intervals of 0.125, increasing in the direction of the arrow. These results are obtained from the dynamic simulations using gPROMS under potentiostatic conditions, by collecting data when the simulations reach steady state. As shown in Fig. 4, the model is well matched with the steady-state trends previously reported in the literature.

3.2. Dynamic behaviour

To verify the dynamic behaviour of the DMFC over the entire operating procedure, a dynamic simulation was performed from start-up to shut-down operation. The total operating time was 1300 s: the start-up (feeding) for 50 s, the normal operation for 750 s, and the shut-down for 500 s (long enough to consume all methanol in the cell). Fig. 5a and b shows the strategies of the power density load and the methanol feeding. At start-up operation, no power is loaded, but 1 M methanol is introduced, and neither methanol feeding nor power loading exists at the shut-down period. During normal operation, 300 W m^{-2} of power density was loaded constantly, and three different concentrations (1.0, 0.5, and 1.5 M) were fed sequentially for an equal period (250 s) to check the effect of methanol feeding on cell performance. Fig. 5c shows the concentration profiles of methanol and carbon dioxide in both the anode compartment and the anode catalyst layer. The methanol concentration tends to vary with the feed concentration; whereas the concentration of carbon dioxide shows a tendency similar to the anode reaction rate shown in Fig. 5d. As soon as the cell enters shut-down operation, the anode reaction rate drops dramatically. By contrast, the methanol crossover flux decreases gradually and results in a steady fall in methanol concentration in both the anode compartment and the anode catalyst layer. This trend indicates that residual methanol remaining after normal operation results only in crossover, which is a waste of fuel. The anode reaction that occurs during the normal operation varies slightly with the concentration of methanol. On the other hand, methanol crossover depends strongly on the concentration of methanol in the anode catalyst layer and exceeds the anode reaction when more methanol is present than required, especially when the cell is in the start-up or the shut-down periods. Consequently, the methanol crossover ratio, which is defined as the ratio of the methanol crossover rate to the sum of the methanol crossover rate and the anode reaction rate, is a maximum in the start-up and shut-down periods, as demonstrated in Fig. 5d. The cell voltage drops suddenly at the early stage of normal operation, and varies with the feeding strategy; it also rises dramatically to reach the open-circuit value in the shut-down period (Fig. 5e). From the dynamic simulation results, it is found that the transient behaviour of the DMFC depends on the feed concentration of methanol and that the performance of the cell can be improved considerably by reducing the amount of methanol crossover, that is, by optimizing the strategy of methanol feeding.

4. Dynamic optimization

4.1. Model formulation

The aim of the dynamic optimization of this research was to find the optimum operating strategies that maximize the performance of the DMFC under a given power density load. The energy efficiency can be a candidate for the objective function to be maximized:

$$\eta_{\text{energy}} = \frac{\int_0^{t_f} U_{\text{cell}}\, i_{\text{cell}}\, A^S \,\mathrm{d}t}{6FU_{\text{cell}}^{\text{STD}} \left(\int_0^{t_f} r_a A^S \,\mathrm{d}t + \int_0^{t_f} n_{\text{MeOH}}^{\text{M}} A^S \,\mathrm{d}t \right)} \tag{23}$$

where t_f means the total operating time of the DMFC system. The numerator of Eq. (23) equals the integral of the power load, which would be constant if the scenario of power load is fixed. Hence, the amount of methanol consumed by the reaction and crossover in the denominator can be used as an alternative to the energy efficiency. By adding the amount of methanol remaining after normal operation is terminated, we formulate the objective function for

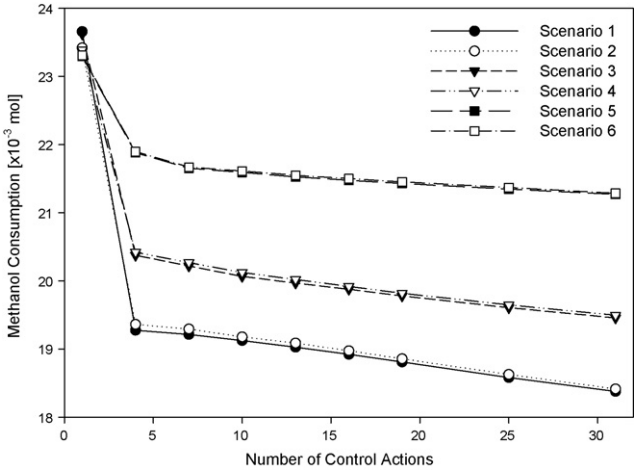

Fig. 6. Summary of 54 optimization results; six scenarios and nine optimizations per scenario varying NCA.

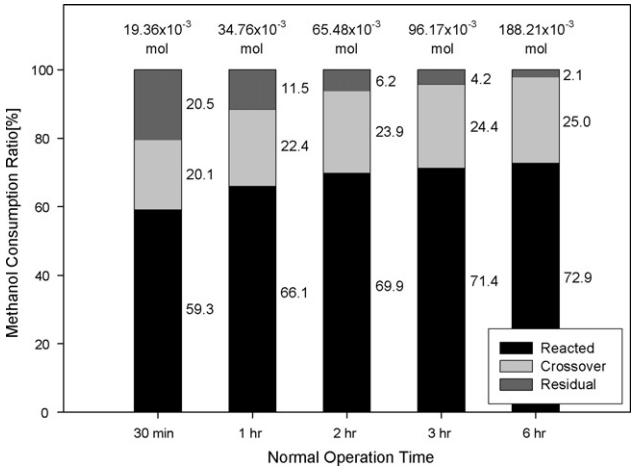

Fig. 7. Variation of methanol consumption ratio with increase in normal operation time; first bar is base case, and total amounts of methanol consumed are indicated by bars.

the dynamic optimization, namely:

$$M_{\mathrm{MeOH}} = \int_0^{t_f} r_a A^S \,\mathrm{d}t + \int_0^{t_f} n^M_{\mathrm{MeOH}} A^S \,\mathrm{d}t + (V_a^{\mathrm{CL}} c^{\mathrm{CL}}_{\mathrm{MeOH}} + V_a c_{\mathrm{MeOH}})|_{t=t_f} \quad (24)$$

here M_{MeOH} is called the amount of methanol consumed, which consists of the amount of methanol reacted, the crossover, and the remainder. The feed concentration is selected as a piecewise constant control variable to be determined. Finally, the dynamic optimization model is formulated as

$$\underset{c^{\mathrm{Feed}}_{\mathrm{MeOH}}}{\mathrm{Min}}\ M_{\mathrm{MeOH}} \ \text{s.t.}\ f(x(t), \dot{x}(t), y(t), v)=0,$$

$$I(x(0), \dot{x}(0), y(0), v)=0,$$

$$\begin{cases} U_{\mathrm{cell}} \geq U^L_{\mathrm{cell}} & @\, t = t_f \\ P_{\mathrm{cell}} = P_{\mathrm{cell,s}} & @\, t_s \leq t \leq t_{s+1}, s = 0, 1, \ \ldots, \mathrm{NS} \\ 0 \leq c^{\mathrm{Feed}}_{\mathrm{MeOH}} \leq 2000\,\mathrm{mol\ m^{-3}} & @\, 0 \leq t \leq t_f \end{cases} \quad (25)$$

where f and I are the model equations and the initial conditions, respectively discussed in Section 2; NS means the number of intervals for the power density load.

4.2. Case study

The purpose of the case study was to determine the influences of (i) the power load and (ii) the number of control actions on the performance of the DMFC system as shown in Fig. 2.

First, six scenarios were generated that considered the real operational phenomena of the system. All scenarios had four steps with a total operation time of 1860 s; Step 1 was the feeding step (60 s) and Steps 2–4 were the normal operation steps (600 s for each step). At Step 1 of each scenario, no power was loaded into the cell. From Steps 2–4, three different types of power density were loaded into the cell without duplication for each scenario: high (460 W m^{-2}), normal (430 W m^{-2}), and low (400 W m^{-2}). Each scenario produced 215 Wh m^{-2} during the operation. Table 3 presents a summary of the six scenarios of the case study.

Second, the performance of DMFC system was also presumed to depend on how many control actions were included. It can be expected that the increase in control actions could enhance the performance of the system. To insure this result, nine dynamic optimizations were performed for each scenario, varying the number of control actions, NCA $\in \{1, 4, 7, 10, 13, 16, 19, 25, 31\}$. NCA = 1 means that methanol is fed optimally in a time-invariant manner. It is assumed that the minimal control interval is 60 s and that every

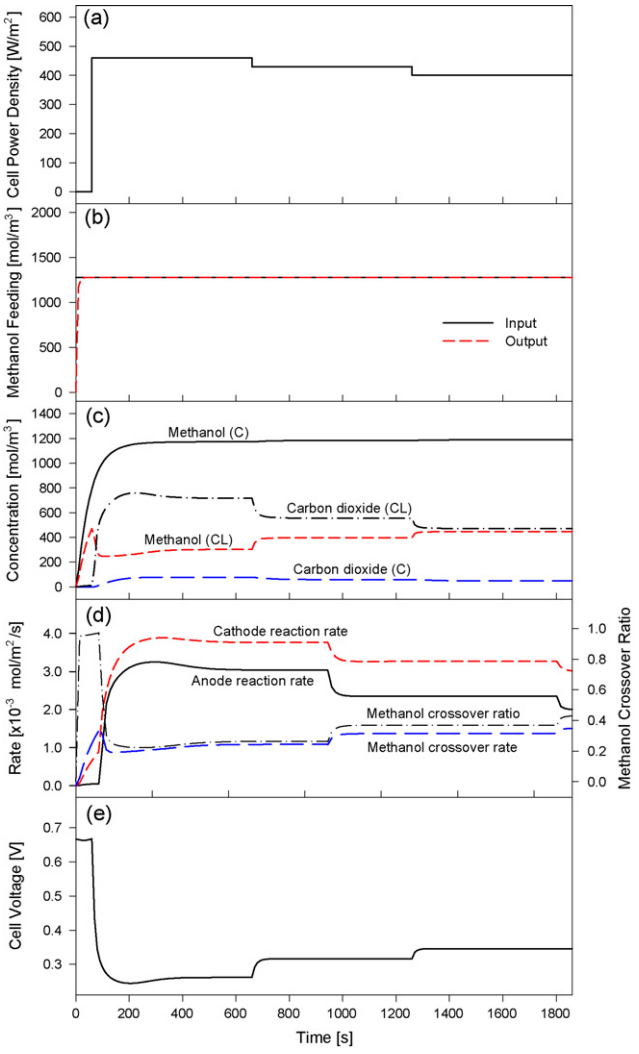

Fig. 8. Transient behaviour of NCA = 1 of Scenario 1. (Subtitles of each graph are same in Fig. 5.)

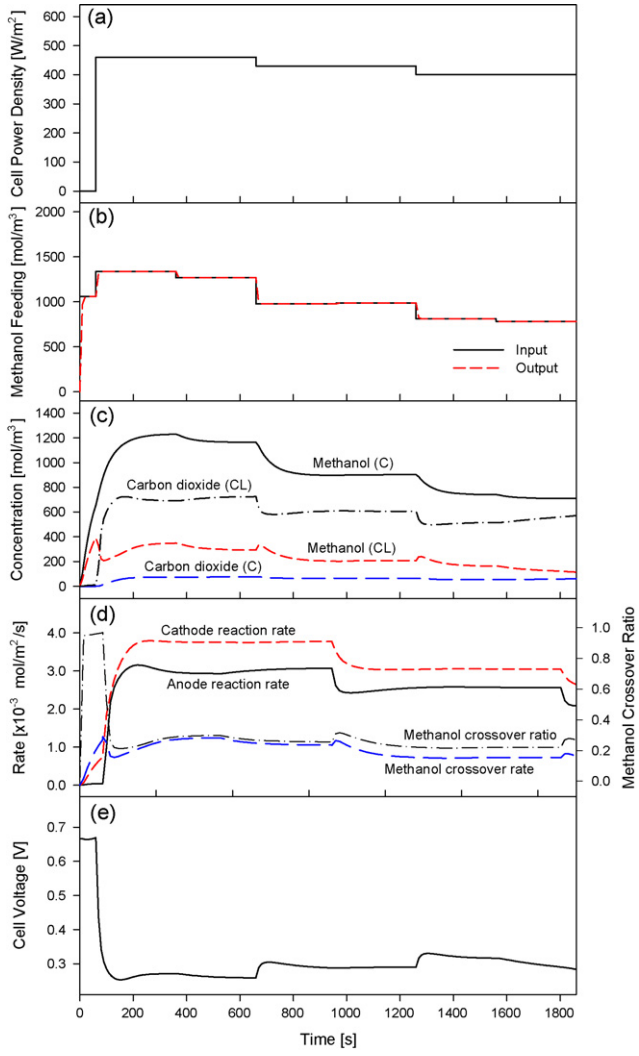

Fig. 9. Transient behaviour of NCA = 7 of Scenario 1. (Subtitles of each graph are same in Fig. 5.)

interval length is the same, except for the feeding step. The feeding step (Step 1) is too short to be divided, but other steps can be divided into up to 10 sections. For example, NCA = 25 means that three steps, except for the feeding step, are divided into eight intervals; the entire operation (1860 s) is thus divided into a 60-s interval and 24 segments of 75-s intervals.

Fig. 6 summarizes the optimaum values of 54 dynamic optimizations (six scenarios and nine optimizations per each scenario). When NCA = 1, the methanol consumptions of each scenario are between 23.3×10^{-3} and 23.7×10^{-3} mol. They drop suddenly according to the last load of power density when NCA = 4. After that, M_{MeOH} decreases gradually as NCA increases in pairs. As can be seen in Fig. 6, the more that the operation is finished with a high load of power density, the more the M_{MeOH} is located at a high position. If two scenarios finish the operation with the same load of power density, the scenario that starts from a lower load of power density consumes slightly less methanol. The reason why methanol consumption depends strongly on the final load of power density is related to the amount of residual methanol, the last term of Eq. (24). To produce high power density, the anode reaction requires an equivalent high concentration of methanol. If the operation ends by producing a high power density, a considerable amount of methanol remains, finally compromising the objective function. This dependence, however, is increasingly weakened as the normal operation time increases. This phenomenon is explained in Fig. 7 in the form of a stacked bar graph and shows the optimaum ratio of methanol consumption as a function of the increase in the normal operation time from 30 min (equal to the case study) to 6 h, applying the power load of Scenario 2. The amount of methanol remaining, which is mainly responsible for the dependence, decreases from 20.5 to 2.1% as the normal operation time increases; whereas the amounts of reacted and crossover methanol increase.

The dynamic behaviour of 54 optimization results can be determined by applying each optimum feeding strategy to the dynamic simulation. To compare the performance of complicated piecewise constant control with the time-invariant control, four optimizations were selected: NCA = 1 and 7 of Scenario 1 (low-ending power load case), and NCA = 1 and 31 of Scenario 5 (high-ending power load case). Figs. 8 and 9 summarize the dynamic behaviour of the optimization results of NCA = 1 and 7 of Scenario 1, respectively. Due to the piecewise constant input of feed concentration, the performance of NCA = 7 is much better than that of NCA = 1; the methanol crossover and final concentration of methanol in the cell are both reduced. Similar results are compared for the high-ending power load scenario in Fig. 10 (NCA = 1 of Scenario 5) and Fig. 11 (NCA = 31 of Scenario 5). The complicated feeding strategy (Fig. 11b) not only

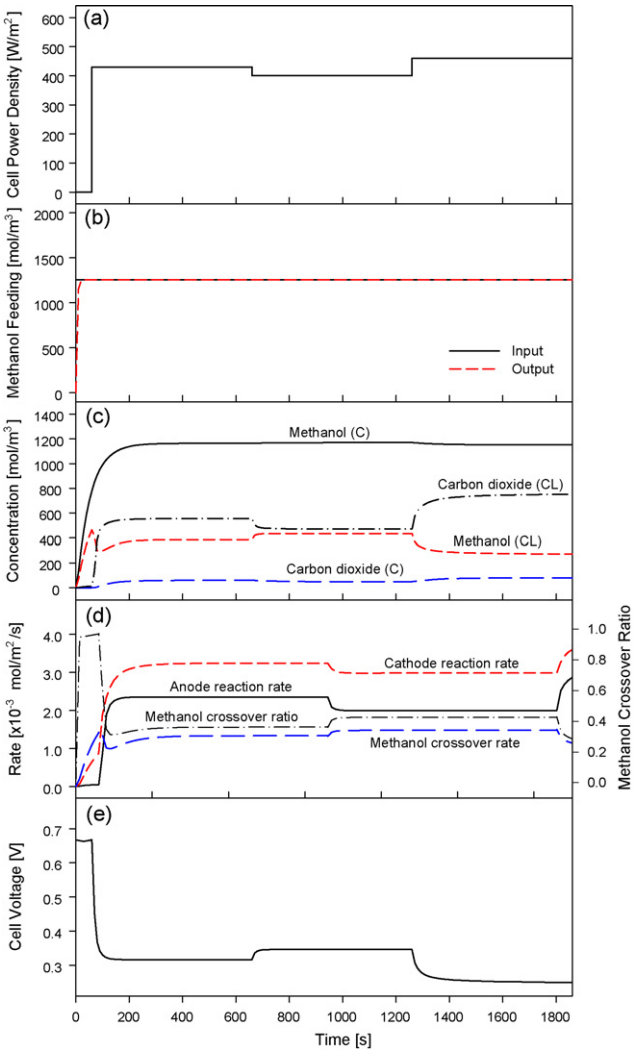

Fig. 10. Transient behaviour of NCA = 1 of Scenario 5. (Subtitles of each graph are same in Fig. 5.)

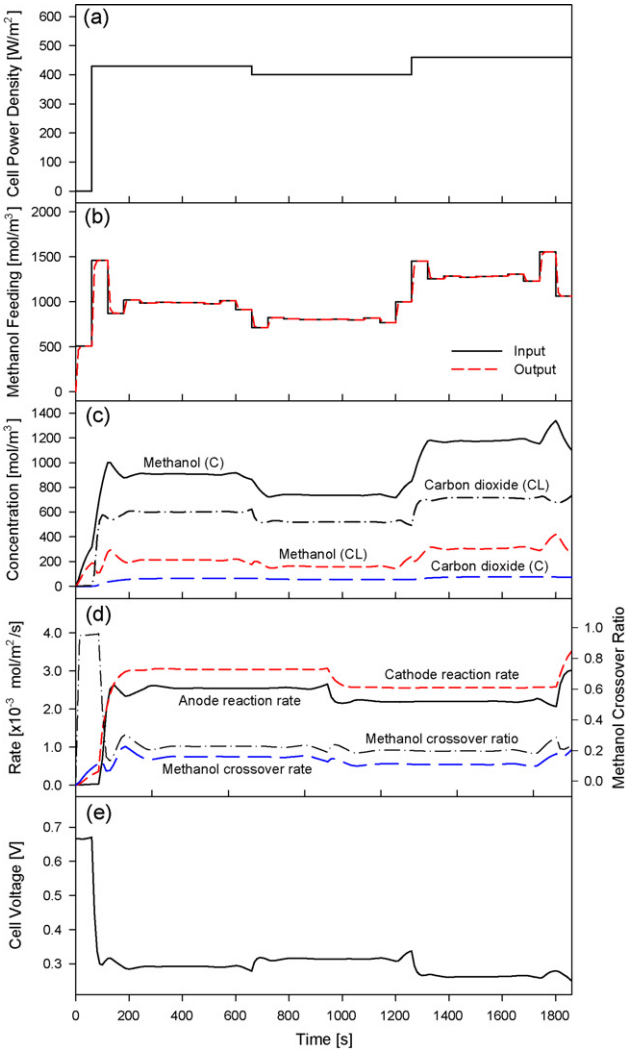

Fig. 11. Transient behaviour of NCA = 31 of Scenario 5. (Subtitles of each graph are same in Fig. 5.)

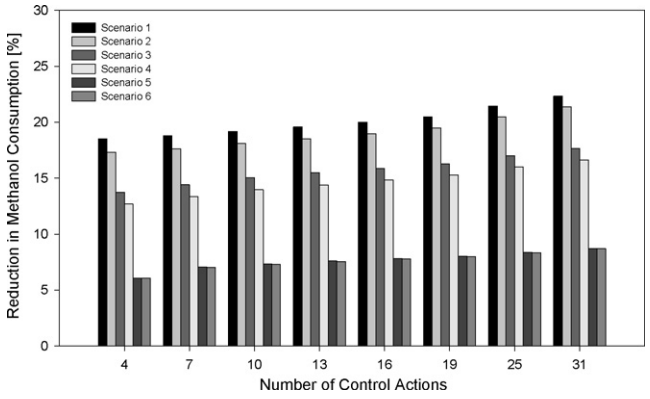

Fig. 12. Reduction in methanol consumption of each control strategy compared with time-invariant control (NCA = 1).

results in fluctuating behaviour of the variables but also exhibits good performance (i.e., low methanol crossover ratio).

Fig. 12 presents the reduction in methanol consumption of each control strategy compared with the time-invariant control (NCA = 1). The more the operation ends with a high power load, the more it reduces methanol consumption. Increasing NCA leads to increasing methanol consumption in the cell. The piecewise constant control of feed concentration reduces the methanol consumption from 18.53 to 22.31% compared with the time-invariant control under Scenario 1, and 6.07–8.69% under Scenario 6.

5. Conclusions

The optimum operating strategies of DMFCs over the entire operation including the start-up and shut-down have been studied. A mathematical model that allows a description of zero initial hold-up conditions is presented as a set of DAEs and verified with experimental data using the parameter estimation method. Steady-state simulation results properly demonstrate the feed concentration dependencies of key variables and dynamic simulation results rigorously explain the transient behaviour of DMFCs. Based on this model, a dynamic optimization problem has been formulated as a non-linear programming (NLP) problem. The methanol consumption, which consists of the amount of methanol reacted, the crossover, and the remainder after operation, is selected as the objective function to be minimized. As a decision variable, the methanol concentration of the anode feed stream is considered in the form of a piecewise constant control. In the case study, six scenarios of power density load are generated to reflect real operational phenomena. By varying the number of control actions, 54 cases of dynamic optimization are performed and compared with each other.

From the case study, it is found that the performance of the DMFC depends on the number of control actions as well as on the power density load. If the overall power generation is the same, the more the operation finishes with a high power density load, the less efficient the system becomes. Increasing the number of control actions reduces methanol consumption, although this requires a complicated control strategy. It is also demonstrated that optimum feeding strategies reduce the feed consumption from 6.07 to 22.31%, depending on the scenario and the number of control actions. In conclusion, the optimum feeding strategies obtained from the dynamic optimizations enabled DMFCs to be operated more efficiently.

Acknowledgements

This work was supported in part by Korea Institute of Science and Technology, and in part by the Ministry of Education, Science and Technology of Korea by its BK21 Program.

References

[1] J.A. Drake, W. Wilson, K. Killeen, J. Electrochem. Soc. 151 (2004) A413–A417.
[2] T.H. Kim, Y.C. Bae, Polymer 46 (2005) 6494–6499.
[3] F. Meier, S. Denz, A. Weller, G. Eigenberger, Fuel Cells 3 (2003) 161–168.
[4] N. Munichandraiah, K. McGrath, G.K.S. Prakash, R. Aniszfeld, G.A. Olah, J. Power Sources 117 (2003) 98–101.
[5] H. Uchida, Y. Mizuno, M. Watanabe, J. Electrochem. Soc. 149 (2002) A682–A687.
[6] Z. Qi, A. Kaufman, J. Power Sources 110 (2002) 177–185.
[7] B. Guraua, E.S. Smotkin, J. Power Sources 112 (2002) 339–352.
[8] V.A. Danilov, J. Lim, I. Moon, H. Chang, J. Power Sources 162 (2006) 992–1002.
[9] K. Sundmacher, T. Schultz, S. Zhou, K. Scott, M. Ginkel, E.D. Gilles, Chem. Eng. Sci. 56 (2001) 333–341.
[10] S. Zhou, T. Schultz, M. Peglowa, K. Sundmacher, Phys. Chem. Chem. Phys. 3 (2001) 347–355.
[11] K.T. Jeng, C.W. Chen, J. Power Sources 112 (2002) 367–375.
[12] T. Schultz, K. Sundmacher, J. Power Sources 145 (2005) 435–462.
[13] U. Krewera, K. Sundmacher, J. Power Sources 154 (2005) 153–170.
[14] C. Xu, P.M. Follmann, L.T. Biegler, M.S. Jhon, Comp. Chem. Eng. 29 (2005) 1849–1860.
[15] D. Ko, M.J. Lee, W.-H. Jang, U. Krewer, J. Power Sources 180 (2008) 71–83.
[16] K. Scott, W. Taama, J. Cruickshank, J. Power Sources 65 (1997) 159–171.
[17] T.E. Springer, T.A. Zawodzinski, S. Gottesfeld, J. Electrochem. Soc. 138 (1991) 2334–2342.
[18] P.S. Kauranen, E. Skou, J. Appl. Electrochem. 26 (1996) 909–917.
[19] X. Ren, W. Henderson, S. Gottesfeld, J. Electrochem. Soc. 144 (1997) L267–L270.
[20] H. Dohle, J. Divisek, R. Jung, J. Power Sources 86 (2000) 469–477.
[21] A. Siebke, W. Schnurnberger, F. Meier, G. Eigenberger, Fuel Cells 3 (2003) 37–47.
[22] Process Systems Enterprise Ltd., gPROMS Introductory User Guide, 2004.
[23] Process Systems Enterprise Ltd., gPROMS Advanced User Guide, 2004.